

# Theory and Analytical Performance Evaluation of Generalized Correlation Beamformers

Anton J. Haug and Garry M. Jacyna

**Abstract**—Traditionally, passive detection and localization of an acoustic source has been based on exploiting the relative differences in temporally averaged power outputs of contiguous beams of an element-weighted beamformer. An alternate approach, the generalized correlation beamformer (GCBF), is proposed where a weighted Toeplitz-averaged (spatially averaged) correlation function is used to estimate the beamformer output power. All element-weight sequences can be transformed into correlation-weight sequences through a convolution operation. Additional weight sequences which cannot be generated from a convolution of real element-weight sequences are available for use in the GCBF. Recently, a special case of the GCBF was proposed by Wilson *et al.* in which the correlation-weights are set to unity, a correlation-weight sequence which cannot be obtained from any classical element-weight sequence. Although such a “boxcar” correlation-weight sequence produces a sharper main peak power response (improved resolution), it has the undesirable effect of producing abnormally high (positive and negative power) sidelobes. General analytical performance bounds are developed that accurately reflect the GCBF detection and bearing localization performance for a noise model that includes spatially white noise and spatially discrete interferers (clutter). Analysis results indicate that the GCBF with Bartlett correlation-weights outperformed the GCBF with unity correlation-weights for both detection and bearing estimation except when the clutter bearing is close to the signal bearing.

**Index Terms**—Beamforming, correlation weighting, generalized correlation beamformer, spatial averaging beamformer, Toeplitz-averaged correlation function.

## I. INTRODUCTION

AS ONE STEP in efforts to improve the performance of sonar systems, proposed new detection and localization algorithms undergo a rigorous analysis process to assess potential performance improvements. This analysis can include the development of analytical performance bounds for each proposed new algorithm, along with a comparison of the performance of the new algorithm with the performance of currently implemented algorithms. The results presented in this paper grew out of such an analysis and represent performance assessments based on a set of rigorously derived detection and bearing estimation performance metrics.

For a linear array of  $M$  hydrophones, choosing the peak averaged power from a bank of unweighted frequency domain phase-delay-and-sum beamformers provides optimal passive detection and estimation when a single signal is present and the

noise is spectrally and spatially white [1]. Element weighting is introduced to reduce the sidelobe response resulting from a finite spatial aperture at the cost of decreased resolution. Averaging over successive fast Fourier transformed (FFT) output samples (snapshots) provides output power estimates for the beamformer. Automatic detection and bearing estimation can then be accomplished by thresholding the power estimates from each beam and choosing only local maxima.

An alternate approach to detection and bearing estimation takes the form of a generalized correlation beamformer (GCBF), where the power in each beam is estimated from the inverse Fourier transform of a weighted single snapshot estimate of the spatial correlation function for all possible pairings of hydrophone elements [2]. The Toeplitz-averaged correlation function provides such an estimate over all possible spatial lags [3]. An element-weighted phase-delay-and-sum beamformer can be transformed into a GCBF, with the correlation-weight sequence generated from the element-weight sequence through a correlation operation. For example, unity element-weights of Bartlett can be transformed into a set of triangular correlation-weights [4]. A second class of correlation-weight sequences gives rise to GCBF responses that cannot be generated from any element-weight sequence. Thus, two classes of correlation-weight sequences can be used with the GCBF: those that can be generated from real element-weight sequences through a convolution operation and those that cannot. For performance comparison purposes, the simplest examples of each class of correlation-weight sequences will be used: Bartlett triangular correlation-weights and Wilson unity correlation-weights [3]. This special case of the GCBF was proposed by Wilson *et al.* [3], [5], [6] and is referred to as the “inverse beamformer” (IBF). Performance metrics for the GCBF are developed throughout this paper using an arbitrary correlation-weight sequence, followed by a specific comparison of the performance for the Bartlett unity element-weight sequence (triangular correlation-weight sequence) with the performance using the Wilson unity correlation-weight sequence.

It is well known that a single snapshot element-weighted phase-delay-and-sum beamformer is the spatial equivalent of the discrete windowed short-time Fourier transform. It will be shown below that the GCBF is the spatial equivalent of the discrete smoothed pseudo-Wigner distribution. With Wilson unity correlation-weights, the GCBF reduces to the spatially discrete version of a Wigner-Ville distribution with the time index set to zero.

In [2], performance metrics for the GCBF were developed assuming the presence of a single spatially discrete signal with

Manuscript received August 13, 1999; revised January 3, 2000.

The authors are with The MITRE Corporation, McLean, VA 22102-3841 USA.

Publisher Item Identifier S 0364-9059(00)05933-1.

element-to-element independent noise. It was further assumed that the probability density function (pdf) of the GCBF output was Gaussian. In this paper, we extend the performance analysis of the GCBF to include interferers (clutter) in the noise model and to evaluate GCBF performance under a more realistic output pdf. With these additions, a set of analytical metrics for evaluating the detection and bearing estimation performance of the GCBF are developed and used to compare the performance of the GCBF using Wilson correlation-weights to its performance using the conventional Bartlett correlation-weights. In all cases, MATLAB programs were used to calculate the performance for a linear array of 48 elements with spacing optimized for the frequency of interest.

Since analytical beamformer performance is dependent on the signal and noise models chosen, Section II defines realistic signal, noise, and interference models. This is followed in Section III by the development of the standard form of the GCBF algorithm from the phase-delay-and-sum beamformer algorithm. A more mathematically compact form of the GCBF, the quadratic form, is then evolved, followed by the derivation of a general expression for the pdf of the GCBF output. Analytical detection performance metrics are then advanced in Section IV, beginning with analytical expressions for the deflection ratio of the GCBF output. The GCBF output deflection ratio for Wilson and Bartlett correlation-weight sequences are computed and compared. Detection performance under the more general assumption of non-Gaussian beamformer output statistics for the two weight sequences are compared through numerical computation of receiver operating characteristic (ROC) curves based on the GCBF output pdfs. In Section V, lower bounds on bearing estimation errors are assessed using two different techniques. First, general expressions for the local rms lower bound on the estimated bearing are developed for the GCBF assuming that the beam containing the signal is chosen in the detection process. These expressions are then used to compare the performance for the two weight sequences. For a more global estimate of bearing error, the probability of choosing an incorrect beam affects the bearing estimation performance. For this case, expressions for the Ziv-Zakai lower bound are developed and used to compare the bearing estimation performance of the two weight sequences. Finally, in Section VI, the performance results are summarized and significant conclusions are presented.

## II. SIGNAL, NOISE, AND INTERFERER MODELS

Assume that the acoustic field is spatially sampled by a discrete linear array of  $M$  elements with inter-element spacing  $d$ . At frequency  $f_0$ , consider an acoustic field with three components: a plane-wave signal of interest arriving from bearing  $\theta_S$  relative to array broadside, multiple plane-wave interference signals from distant spatially discrete acoustic sources with the  $l$ th interference signal arriving from bearing  $\theta_l$  relative to array broadside, and distributed noise. We define the *normalized wavenumber*  $k$  as

$$k \equiv 2\pi d/\lambda_0 \quad (1)$$

where  $\lambda_0 \equiv c/f_0$  and the speed of sound in water is  $c$ . We define  $u$  as

$$u \equiv \sin \theta \quad (2)$$

with  $-\pi/2 \leq \theta \leq \pi/2$ .

The complex output at frequency  $f_0$  after a Fourier transform operation on the  $m$ th hydrophone data can be written as

$$x_m \equiv s_m + t_m + v_m \quad (3)$$

where the contribution from the signal of interest is given by

$$s_m \equiv \alpha_S e^{jkmu_S} \quad (4)$$

and the contribution from discrete interferers is given by

$$t_m \equiv \sum_{l=1}^L \alpha_l e^{jkmu_l} \quad (5)$$

Assume that  $v_m$ ,  $\alpha_S$ , and  $\alpha_l$  are complex zero-mean Gaussian random variables that are independent of each other for all  $m$  and  $l$ . Also assume that the magnitude of any signal from a spatially discrete source (signal or interferer) is constant across the array for any given observational interval. The noise contribution term  $v_m$  is defined as spatially white noise that is element-to-element independent, so that

$$\langle v_m v_{m'}^* \rangle = \langle |v_m|^2 \rangle \delta_{mm'} \equiv \sigma_N^2 \delta_{mm'} \quad (6)$$

where  $\langle \cdot \rangle$  represents the expected value and  $\delta_{mm'}$  is the Kronecker delta function defined by

$$\delta_{mm'} \equiv \begin{cases} 1, & m = m' \\ 0, & m \neq m'. \end{cases} \quad (7)$$

Forming the pairwise correlation-products  $x_m x_{m'}^*$  that are elements of the data correlation-product matrix  $\mathcal{R}$ , we can write

$$\begin{aligned} \rho(m - m') &\equiv x_m x_{m'}^* \\ &= \alpha_S \alpha_S^* e^{jk(m-m')u_S} \\ &\quad + \alpha_S \sum_{l=1}^L \alpha_l^* e^{jk(mu_S - m'u_l)} + \alpha_S e^{jkmu_S} v_m^* \\ &\quad + \sum_{l=1}^L \alpha_l \alpha_S^* e^{jk(mu_l - m'u_S)} \\ &\quad + \sum_{l=1}^L \sum_{l'=1}^L \alpha_l \alpha_{l'}^* e^{jk(mu_l - m'u_{l'})} \\ &\quad + \sum_{l=1}^L \alpha_l e^{jkmu_l} v_m^* + v_m \alpha_S^* e^{-jkmu_S} \\ &\quad + v_m \sum_{l=1}^L \alpha_l^* e^{-jkmu_l} + v_m v_m^*. \end{aligned} \quad (8)$$

We define the spatial lag  $p$  as

$$p \equiv m - m'. \quad (9)$$

Note that, since  $m$  and  $m'$  take on values  $\{0, 1, \dots, M-1\}$ ,  $p$  has the range  $\{-(M-1), \dots, -1, 0, 1, \dots, M-1\}$ . Thus,

$$\langle \rho(p) \rangle = \sigma_S^2 e^{jkpu_S} + \sum_{l=1}^L \sigma_l^2 e^{jkpu_l} + \sigma_N^2 \delta(p) \quad (10)$$

where, since  $\alpha_S$  and  $\alpha_I$  are complex zero-mean Gaussian processes, the signal and interferer average powers are given by  $\sigma_S^2 \equiv \langle |\alpha_S|^2 \rangle$  and  $\sigma_I^2 \equiv \langle |\alpha_I|^2 \rangle$ .

The zero-mean complex random amplitudes for the signal, clutter, and noise from (4)–(6) can be written in complex notation as  $\alpha_S = \alpha_S^r + j\alpha_S^i$ ,  $\alpha_I = \alpha_I^r + j\alpha_I^i$ , and  $v_l = v_l^r + jv_l^i$ , respectively, with  $\langle \alpha_S^r \alpha_S^i \rangle = 0$ ,  $\langle \alpha_I^r \alpha_I^i \rangle = 0$  ( $\forall l, l'$ ), and  $\langle v_m^r v_m^i \rangle = 0$  ( $\forall m, m'$ ). Note that both the real and imaginary components of each amplitude are zero-mean since the complex amplitudes are zero-mean. Also,

$$\langle \alpha_S^r \alpha_S^r \rangle = \langle \alpha_S^i \alpha_S^i \rangle = \langle \sigma_S^2 / 2 \rangle, \quad (11)$$

$$\langle \alpha_I^r \alpha_I^r \rangle = \langle \alpha_I^i \alpha_I^i \rangle = \langle \sigma_I^2 / 2 \rangle \delta_{ll'}, \quad (12)$$

and

$$\langle v_m^r v_{m'}^r \rangle = \langle v_m^i v_{m'}^i \rangle = \langle \sigma_N^2 / 2 \rangle \delta_{mm'}. \quad (13)$$

### III. GENERALIZED CORRELATION BEAMFORMER

#### A. Standard Form of the Generalized Correlation Beamformer

The power output  $b_c$  from a conventional frequency-domain beamformer steered in the direction  $\theta_0$  is given by [1], [7]

$$b_c(u_0) = \sum_{m=0}^{M-1} \sum_{m'=0}^{M-1} g_m g_{m'}^* \langle x_m x_{m'}^* \rangle e^{jk(m-m')u_0} \quad (14)$$

where  $g_m$  is a weight (element-weight) applied to the output of the  $m$ th element and  $u_0 = \sin \theta_0$ . Converting (14) to quadratic form results in

$$b_c(u_0) = \mathbf{w}^H \mathbf{R} \mathbf{w} \quad (15)$$

where the complex elements of  $\mathbf{w}$  are given by

$$w_m = g_m e^{jk m u_0} \quad (16)$$

and the complex elements of the correlation matrix  $\mathbf{R}$  are given by

$$R_{mm'} = \langle \rho(m-m') \rangle = \langle x_m x_{m'}^* \rangle. \quad (17)$$

The beamformer output power can be estimated in one of two ways. First,  $b_c(u_0)$  can be computed using (14), replacing  $\langle x_m x_{m'}^* \rangle$  by its single snapshot equivalent  $x_m x_{m'}^*$  (elements of the data correlation-product matrix  $\mathcal{R}$ ), and averaging the beamformer output over successive snapshots. Here, a snapshot is defined as a single FFT output for all elements. Alternately, the elements of  $\mathbf{R}$  can be estimated by averaging  $\mathcal{R}$  over successive snapshots and using the elements of the averaged  $\mathcal{R}$  in place of the elements of  $\mathbf{R}$  in (14).

Using the definition of  $p$  from (9), (14) can be rewritten as

$$\begin{aligned} b_c(u_0) &= \sum_{p=-(M-1)}^{-1} \sum_{m=0}^{M-1+p} g_m g_{m-p}^* \langle x_m x_{m-p}^* \rangle e^{-jk p u_0} \\ &+ \sum_{m=0}^{M-1} |g_m|^2 \langle x_m x_m^* \rangle \\ &+ \sum_{p=1}^{M-1} \sum_{m=0}^{M-1-p} g_m g_{m+p}^* \langle x_m x_{m+p}^* \rangle e^{jk p u_0}. \end{aligned} \quad (18)$$

From (10), it can be noted that all elements of the  $p$ th diagonal of  $\mathbf{R}$  will have the same signal component, independent of the value of  $m$  or  $m'$ . Therefore, an alternate estimate of  $\langle x_m x_{m \pm p}^* \rangle$  can be obtained from a single snapshot of the data record by computing the spatial average along each diagonal of the data correlation matrix  $\mathcal{R}$  [4, eq. 5.9]. Defining the Toeplitz-averaged correlation function  $C(p)$  as an estimate of  $\langle x_m x_{m \pm p}^* \rangle$ ,  $C(p)$  can be calculated from [2], [3, eq. 9] as

$$C(p) = \frac{1}{M-|p|} \sum_{m=0}^{M-1-|p|} x_m x_{m+|p|}^*, \quad 0 \leq |p| \leq M-1. \quad (19)$$

Hence, an alternate estimate of the average beamformer power output can be obtained from (18) by substitution of the Toeplitz-averaged correlation function at lag  $p$  for each diagonal element of  $\mathbf{R}$  at lag  $p$ , resulting in

$$b_c(u_0) = \sum_{p=-(M-1)}^{M-1} h_c(p) C(p) e^{jk p u_0} \quad (20)$$

where the correlation-weight sequence  $h_c(p)$  has been obtained from the conventional beamformer element-weight sequence  $g_m$  using a convolution operation as follows:

$$h_c(p) = \begin{cases} \sum_{m=0}^{M-1-p} g_m g_{m+p}^*, & 0 \leq p \leq M-1 \\ h_c(-p), & -(M-1) \leq p < 0. \end{cases} \quad (21)$$

When a uniform element-weight sequence is used,  $g_m = 1$ , and (21) reduces to the Bartlett correlation-weight sequence:  $h_B(p) = 1 - (|p|/M)$ . Equation (20) can be generalized to include correlation-weight sequences that cannot be generated from the element-weight sequence transformation given by (21). One such correlation-weight sequence is the Wilson weight sequence,  $h_W(p) = 1$  [3]. Thus, (20) can be rewritten as the *generalized correlation beamformer* (GCBF)

$$b(u_0) = \sum_{p=-(M-1)}^{M-1} h(p) C(p) e^{jk p u_0} \quad (22)$$

with

$$h(p) = \begin{cases} h_c(p) & \text{Conventional weight sequence} \\ h_B(p) & \text{Bartlett weight sequence} \\ 1 & \text{Wilson weight sequence.} \end{cases} \quad (23)$$

Note that, for all cases,  $h(p)$  is symmetric about  $p = 0$ , and, since  $h(p)$  is a correlation sequence, it is normalized such that  $h(0) = 1$ .

The GCBF can be identified as a spatial version of the discrete smoothed pseudo-Wigner distribution [1], [8, eq. 60]

$$W(n, \omega) = \sum_{p=-(M-1)}^{M-1} w(p) R(p, n) e^{j p \omega} \quad (24)$$

with the time index  $n$  set to 0, the frequency index  $\omega$  replaced by  $k u_0$ , and the correlation product  $R(p, 0)$  replaced by the estimate  $C(p)$ .

### B. Quadratic Form of the Generalized Correlation Beamformer

For narrow-band signal and noise processes,  $x_m$  is the complex output of the data Fourier transform from the  $m$ th sensor for an implied frequency  $f_0$ . Thus, we can write  $x_m \equiv x_m^r + jx_m^i$  so that

$$x_m x_{m+p}^* = (x_m^r x_{m+p}^r + x_m^i x_{m+p}^i) + j(x_m^r x_{m+p}^i - x_m^i x_{m+p}^r). \quad (25)$$

Since  $C(p)$  is complex,  $C(p) = C_r(p) + jC_i(p)$ . From (19), using (25), for  $0 \leq p \leq M-1$ , we can write

$$C_r(p) = \frac{1}{M-p} \sum_{m=0}^{M-1-p} x_m^r x_{m+p}^r + \frac{1}{M-p} \sum_{m=0}^{M-1-p} x_m^i x_{m+p}^i \quad (26)$$

and

$$C_i(p) = \frac{1}{M-p} \sum_{m=0}^{M-1-p} x_m^r x_{m+p}^i - \frac{1}{M-p} \sum_{m=0}^{M-1-p} x_m^i x_{m+p}^r. \quad (27)$$

Now, (22) can be expanded as follows:

$$\begin{aligned} b(u_0) &= h(0)C(0) + \sum_{p=-(M+1)}^{M-1} h(p)C_r(p) \cos(kpu_0) \\ &\quad - \sum_{p=-(M+1)}^{M-1} h(p)C_i(p) \sin(kpu_0). \end{aligned} \quad (28)$$

We define the *real-valued* data vector to be

$$\mathbf{x}^T \equiv \{x_0^r, x_1^r, \dots, x_{M-1}^r, x_0^i, x_1^i, \dots, x_{M-1}^i\}. \quad (29)$$

Using (26), (27) and (29), (28) can be written in the quadratic form

$$b(\theta_0) = \mathbf{x}^T \mathbf{D}(\theta_0) \mathbf{x} \quad (30)$$

with

$$\mathbf{D}(\theta_0) = \begin{pmatrix} D_1(\theta_0) & D_2(\theta_0) \\ -D_2(\theta_0) & D_1(\theta_0) \end{pmatrix}. \quad (31)$$

Here,  $D_1(\theta_0)$  is given by the symmetric Toeplitz matrix

$$\begin{aligned} D_1(\theta_0) &= \begin{pmatrix} d_{10}(\theta_0) & d_{11}(\theta_0) & \cdots & d_{1(M-1)}(\theta_0) \\ d_{11}(\theta_0) & d_{12}(\theta_0) & \cdots & d_{1(M-2)}(\theta_0) \\ \vdots & \vdots & \ddots & \vdots \\ d_{1(M-1)}(\theta_0) & d_{1(M-2)}(\theta_0) & \cdots & d_{10}(\theta_0) \end{pmatrix} \end{aligned} \quad (32)$$

with elements

$$d_{1p}(\theta_0) = \frac{1}{M-|p|} h(p) \cos(kpu_0) \quad (33)$$

and  $D_2(\theta_0)$  is given by the skew symmetric Toeplitz matrix

$$D_2(\theta_0) = \begin{pmatrix} 0 & d_{21}(\theta_0) & \cdots & d_{2(M-1)}(\theta_0) \\ -d_{21}(\theta_0) & 0 & \cdots & d_{2(M-2)}(\theta_0) \\ \vdots & \vdots & \ddots & \vdots \\ -d_{2(M-1)}(\theta_0) & -d_{2(M-2)}(\theta_0) & \cdots & 0 \end{pmatrix} \quad (34)$$

with elements

$$d_{2p}(\theta_0) = \frac{1}{M-|p|} h(p) \sin(kpu_0). \quad (35)$$

Note that  $D_2(\theta_0)$  is skew symmetric because  $\sin(kpu_0)$  is an odd function of  $p$ . Note also that the eigenvalues of  $\mathbf{D}$  are not necessarily all positive, since  $\mathbf{D}$  contains the correlation-weight coefficients, and that the sum of the eigenvalues can be negative giving rise to negative beamformer output responses.

The normalized responses of the GCBF with Bartlett and Wilson correlation-weight sequences for two different signal directions are shown in Figs. 1 and 2 ( $\theta_0 = 0$  and 80 degrees, respectively.) For both figures, the beam steering direction is fixed but the signal is swept in bearing. Thus, the bearing axis represents the response to a signal at that bearing. Two obvious conclusions can be drawn from the two plots: Wilson weights show a more oscillatory response than Bartlett weights do with negative responses for many bearings, and Wilson weights have a narrower main lobe response than Bartlett weights. The first conclusion implies increased sidelobe leakage at many bearings for the Wilson weights and, thus, a potential for a decrease in detection capability when clutter is present in the sidelobes. The second conclusion implies that the GCBF with Wilson correlation-weights has better resolution in the look direction and the ability to resolve closely spaced targets. This appears to be the primary advantage to using Wilson correlation-weights rather than the more conventional Bartlett correlation-weights, as has been pointed out previously [2], [3], [5], [6], [9]–[11].

For the noise-free case when two signals (or a signal and an interferer) are present at different bearings, the instantaneous output of a continuum of beams whose maximum response axes (look direction) spans  $-\pi/2 \leq \theta_0 \leq \pi/2$  will exhibit cross terms at look directions between the signal bearings. Fig. 3 presents the GCBF response for both Wilson and Bartlett correlation-weights for two deterministic signals placed at 0 and 5 degrees. The bearing axis now corresponds to the beam steering angle or look direction. For the Bartlett weights, the response from the beam containing the cross terms is suppressed by the weight sequence, which acts as a spatial filter suppressing the response to the two signals in the sidelobes. Since the Wilson weights are unity, the cross terms generate additional response peaks in beams centered at bearings between the two signal bearings. For closely spaced signals, these additional response peaks can exceed the response at the signal bearings [1], resulting in false detections in other beams. This is entirely consistent with identification of the GCBF as a spatial version of the discrete pseudo-Wigner distribution. Such cross-term components have been observed in the presence of two or more

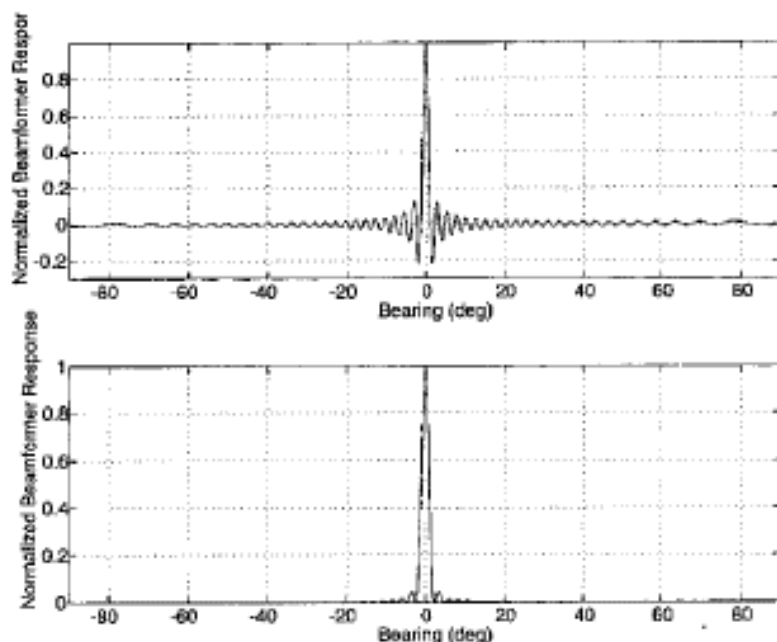


Fig. 1. Normalized GCBF response for a broadside look direction. Top: Wilson weights. Bottom: Bartlett weights.

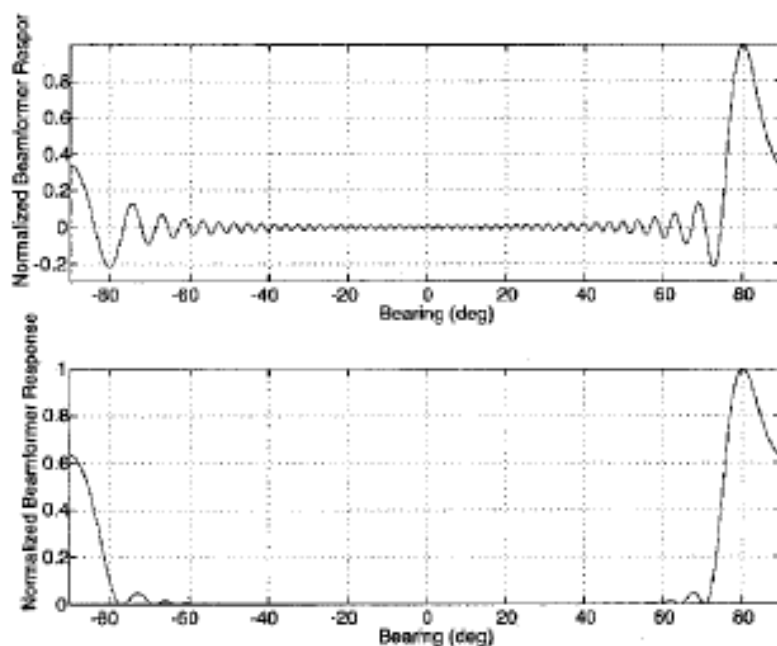


Fig. 2. Normalized GCBF response for a look direction of 80 degrees. Top: Wilson weights. Bottom: Bartlett weights.

signals when unity correlation-weight sequences have been used [1].

### C. The Probability Density Function of the GCBF Output

The quadratic form of the conventional beamformer in (15) shows that the data correlation-product matrix  $\mathcal{R}$  is averaged over many snapshots to generate an estimate of the correlation matrix  $R$ . Since the temporal averaging is on each correlation-product separately, the variance of each element of  $R$

will be the same, allowing the probability distribution of  $b$  in (15) to be determined from the central limit theorem applied to the joint-probability distribution of the components of  $R$ . In the GCBF, on the other hand,  $C(p)$ , the Toeplitz-averaged correlation function, is generated by the spatial averaging of correlation-products with the same lag within each snapshot. Since the number of correlation-products summed in (19) varies with the lag value, the variance of  $C(p)$  will be a function of  $p$  and the central limit theorem will not apply to the probability distribution of  $b$  in (30) relative to the joint-probability distribution of

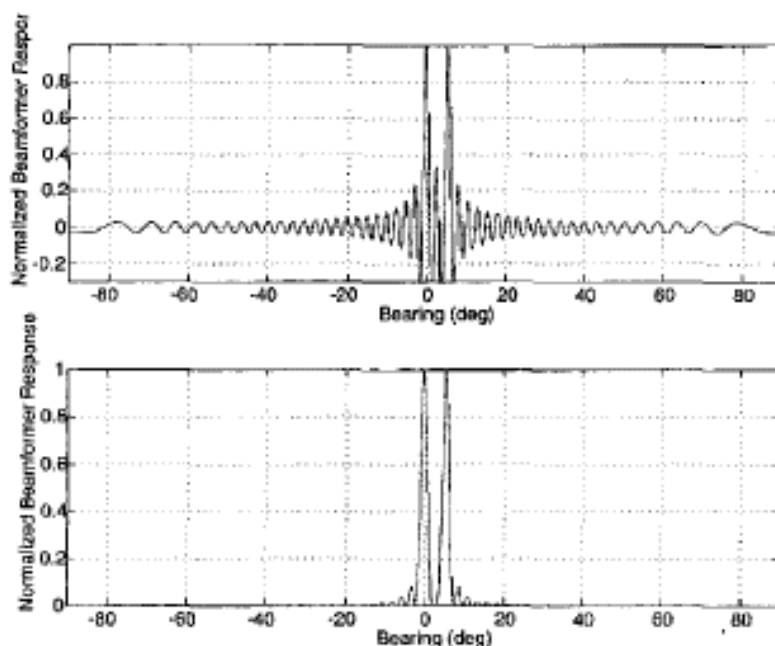


Fig. 3. Comparison of GCBF instantaneous response with: (top) Bartlett and (bottom) Wilson weights for a two-signal case.

the components of  $C(p)$ . Thus, an alternate approach must be developed to obtain the pdf of  $h$ .

Let  $H_q$  represent the hypothesis that signal, noise, and clutter are all present when  $q = 1$  and that only noise and clutter are present when  $q = 0$ . Under  $H_1$ , the components of the data vector  $\mathbf{x}$  can be decomposed into their real and imaginary parts as follows:

$$\begin{aligned} x_m^r &= \alpha_S^r \cos(kmu_S) - \alpha_S^i \sin(kmu_S) \\ &+ \sum_{l=1}^L \alpha_l^r \cos(kmu_l) - \sum_{l=1}^L \alpha_l^i \sin(kmu_l) + v_m^r \end{aligned} \quad (36)$$

$$\begin{aligned} x_m^i &= \alpha_S^i \cos(kmu_S) + \alpha_S^r \sin(kmu_S) \\ &+ \sum_{l=1}^L \alpha_l^i \cos(kmu_l) + \sum_{l=1}^L \alpha_l^r \sin(kmu_l) + v_m^i. \end{aligned} \quad (37)$$

Clearly,  $\langle x_m^r | H_0 \rangle = \langle x_m^i | H_0 \rangle = 0$  (zero mean).

Defining

$$\zeta_p \equiv (2/\sigma_N^2) \langle x_m^r x_{m+p}^r | H_1 \rangle = (2/\sigma_N^2) \langle x_m^i x_{m+p}^i | H_1 \rangle \quad (38)$$

and

$$\varepsilon_p \equiv (2/\sigma_N^2) \langle x_m^r x_{m+p}^i | H_1 \rangle = -(2/\sigma_N^2) \langle x_m^i x_{m+p}^r | H_1 \rangle \quad (39)$$

then

$$\zeta_p = \text{SNR} \cdot \cos(kpu_S) + \sum_{l=1}^L \text{INR}_l \cos(kpu_l) + \delta_{p0} \quad (40)$$

and

$$\varepsilon_p = \text{SNR} \cdot \sin(kpu_S) + \sum_{l=1}^L \text{INR}_l \sin(kpu_l) \quad (41)$$

with the signal-to-noise ratio (SNR) defined by  $\text{SNR} \equiv (\sigma_S^2/\sigma_N^2)$  and the interferer-to-noise ratio (INR) defined by  $\text{INR}_l \equiv (\sigma_l^2/\sigma_N^2)$ . Under  $H_0$ ,  $\text{SNR} = 0$ .

Then, the correlation matrix  $R_q$ , under  $H_q$ , is

$$R_q \equiv \langle \mathbf{x}\mathbf{x}^T | H_q \rangle = \frac{\sigma_N^2}{2} \begin{pmatrix} \mathbf{A}_{1q} & \mathbf{A}_{2q} \\ -\mathbf{A}_{2q} & \mathbf{A}_{1q} \end{pmatrix} \quad (42)$$

where  $\mathbf{A}_{1q}$  is a symmetric Toeplitz matrix given by

$$\mathbf{A}_{1q} \equiv \begin{pmatrix} \zeta_0 & \zeta_1 & \cdots & \zeta_{M-1} \\ \zeta_1 & \zeta_0 & \cdots & \zeta_{M-2} \\ \vdots & \vdots & \ddots & \vdots \\ \zeta_{M-1} & \zeta_{M-2} & \cdots & \zeta_0 \end{pmatrix} \quad (43)$$

and  $\mathbf{A}_{2q}$  is a skew symmetric Toeplitz matrix given by

$$\mathbf{A}_{2q} \equiv \begin{pmatrix} 0 & \varepsilon_1 & \cdots & \varepsilon_{M-1} \\ -\varepsilon_1 & 0 & \cdots & \varepsilon_{M-2} \\ \vdots & \vdots & \ddots & \vdots \\ -\varepsilon_{M-1} & -\varepsilon_{M-2} & \cdots & 0 \end{pmatrix}. \quad (44)$$

Note that the dependence of  $R_q$ ,  $\mathbf{A}_{1q}$ , and  $\mathbf{A}_{2q}$  on  $\theta_0$  has been suppressed and, under  $H_1$ , they are also dependent on  $\theta_S$ . In the analysis that follows, our goal is a comparison of the bounds on performance for the case where the signal is at array broadside; thus,  $\theta_S = 0 \rightarrow u_S = 0$  leads to  $\mathbf{A}_{11} = (\text{SNR})\mathbf{1}\mathbf{1}^T + \mathbf{A}_{10}$ , and  $\mathbf{A}_{21} = \mathbf{A}_{20}$ , with  $\mathbf{1} \equiv (1, 1, \dots, 1)^T$ .

Since  $\mathbf{x}$  is composed of real-valued zero-mean Gaussian random variables, the pdf of  $\mathbf{x}$  conditioned on  $H_q$  is given by

$$p(\mathbf{x} | H_q) = (1/2\pi)^M |R_q|^{-1/2} e^{-(1/2)\mathbf{x}^T R_q^{-1} \mathbf{x}}. \quad (45)$$

From (30),  $b(\theta_0)$  is a function of  $\mathbf{x}$  and, thus, the characteristic function  $\Phi_{b(\theta_0)}(\omega|H_0) \equiv \langle e^{-j\omega b(\theta_0)} \rangle$ , associated with the pdf of  $b(\theta_0)$ , is given by [14]

$$\Phi_{b(\theta_0)}(\omega|H_0) = \int \cdots \int_{-\infty}^{\infty} e^{-j\omega b(\theta_0)} p(\mathbf{x}|H_0) d\mathbf{x} \\ = |\mathbf{I} + 2j\omega \mathbf{D}(\theta_0) \mathbf{R}_0|^{-1/2}. \quad (46)$$

Note that our definition of the characteristic function is the Fourier transform of the pdf vice the standard inverse Fourier transform definition. We do this to conform to the developments in [12], [14]. Since the matrix product  $\mathbf{D}(\theta_0) \mathbf{R}_0$  is not symmetric, its spectral decomposition is given by a singular value decomposition as follows:

$$\mathbf{D}(\theta_0) \mathbf{R}_0 = \mathbf{U}_q \mathbf{\Lambda}_q(\theta_0) \mathbf{V}_q^T \quad (47)$$

where  $\mathbf{U}_q$  is a matrix of eigenvectors for  $[\mathbf{D}(\theta_0) \mathbf{R}_0][\mathbf{D}(\theta_0) \mathbf{R}_0]^T$ ,  $\mathbf{V}_q$  is a matrix of eigenvectors for  $[\mathbf{D}(\theta_0) \mathbf{R}_0]^T[\mathbf{D}(\theta_0) \mathbf{R}_0]$ , and the matrix of corresponding eigenvalues is

$$\mathbf{\Lambda}_q(\theta_0) = \begin{pmatrix} \lambda_{1q}(\theta_0) & & & 0 \\ & \lambda_{2q}(\theta_0) & & \\ & & \ddots & \\ \mathbf{0}^T & & & \lambda_{2Mq}(\theta_0) \end{pmatrix}. \quad (48)$$

Then

$$\mathbf{I} + 2j\omega \mathbf{D}(\theta_0) \mathbf{R}_0 = \mathbf{I} + 2j\omega \mathbf{U}_q \mathbf{\Lambda}_q(\theta_0) \mathbf{V}_q^T \\ = \mathbf{U}_q (\mathbf{I} + 2j\omega \mathbf{\Lambda}_q(\theta_0)) \mathbf{V}_q^T. \quad (49)$$

Since both  $\mathbf{U}_q$  and  $\mathbf{V}_q$  are unitary, i.e.,  $|\mathbf{U}_q| = |\mathbf{V}_q| = 1$ , we obtain

$$|\mathbf{I} + 2j\omega \mathbf{D}(\theta_0) \mathbf{R}_0| = |\mathbf{I} + 2j\omega \mathbf{\Lambda}_q(\theta_0)| \\ = \prod_{k=1}^{2M} (1 + 2j\omega \lambda_{kq}(\theta_0)), \quad (50)$$

and

$$\Phi_{b(\theta_0)}(\omega|H_0) = \prod_{k=1}^{2M} (1 + 2j\omega \lambda_{kq}(\theta_0))^{-1/2}. \quad (51)$$

The pdf corresponding to  $b(\theta_0)$  is determined by integrating  $\Phi_{b(\theta_0)}(\omega|H_0)$  according to

$$p(b(\theta_0)|H_0) = \frac{1}{2\pi} \int_{-\infty}^{\infty} \Phi_{b(\theta_0)}(\omega|H_0) e^{j\omega b(\theta_0)} d\omega. \quad (52)$$

When a closed-form solution does not exist, (52) can be integrated numerically to obtain the pdf's. Several examples of ROC curves for numerically integrated pdf's are presented in Section IV-C. Under certain restrictive assumptions, closed-form solutions to (52) exist. It can be shown [16] that, for the noise-only case (no signal or clutter) and the array steered to broadside, the GCBF output of  $b(0)$  with *Bartlett*

correlation-weights is  $\chi^2$  distributed with two degrees of freedom. With *Wilson* correlation-weights, the output is a *mixture* distribution composed of the weighted sum of symmetric  $\chi^2$  distributions, each with two degrees of freedom.

#### IV. DETECTION PERFORMANCE OF THE GCBF

##### A. Deflection Ratio for the GCBF

The deflection ratio  $D_f(\theta_0, \theta_S)$  for an array steered to  $\theta_0$  is the change in  $b$  in the presence of the signal, normalized by the standard deviation of  $b$  under noise. It is a measure of the SNR at the output of the GCBF and is defined by [1]

$$D_f(\theta_0, \theta_S) \equiv \frac{\langle b(\theta_0)|H_1 \rangle - \langle b(\theta_0)|H_0 \rangle}{\sqrt{\text{Var}(b(\theta_0)|H_0)}}. \quad (53)$$

Now

$$\langle b(\theta_0)|H_0 \rangle = \langle \mathbf{x}^T \mathbf{D}(\theta_0) \mathbf{x} | H_0 \rangle = \text{Trace}(\mathbf{D}(\theta_0) \mathbf{R}_0). \quad (54)$$

Then, using (31) and (42),

$$\langle b(\theta_0)|H_0 \rangle = \sigma_N^2 \text{Trace}[\mathbf{D}_1(\theta_0) \mathbf{A}_{1q} - \mathbf{D}_2(\theta_0) \mathbf{A}_{2q}]. \quad (55)$$

In addition,

$$\langle b^2(\theta_0)|H_0 \rangle = \langle \mathbf{x}^T \mathbf{D}(\theta_0) \mathbf{x} \mathbf{x}^T \mathbf{D}(\theta_0) \mathbf{x} | H_0 \rangle \\ = \sum_{i,j} \sum_{k,l} D_{ij}(\theta_0) D_{kl}(\theta_0) \langle x_i x_j x_k x_l | H_0 \rangle. \quad (56)$$

Since  $x_i$  is composed of real-valued zero-mean Gaussian random variables,<sup>1</sup>

$$\langle x_i x_j x_k x_l | H_0 \rangle = R_{0ij} R_{0kl} + R_{0ik} R_{0jl} + R_{0jk} R_{0il} \quad (57)$$

and (56) becomes

$$\langle b^2(\theta_0)|H_0 \rangle = [\text{Trace}(\mathbf{D}(\theta_0) \mathbf{R}_0)]^2 + 2 \text{Trace} [(\mathbf{D}(\theta_0) \mathbf{R}_0)^2]. \quad (58)$$

Thus, we can write

$$\text{Var}(b(\theta_0)|H_0) \\ = \langle b^2(\theta_0)|H_0 \rangle - \langle b(\theta_0)|H_0 \rangle^2 \\ = 2 \text{Trace} [(\mathbf{D}(\theta_0) \mathbf{R}_0)^2] \\ = \sigma_N^4 \text{Trace} \{[\mathbf{D}_1(\theta_0) \mathbf{A}_{10} - \mathbf{D}_2(\theta_0) \mathbf{A}_{20}]^2\} \\ - \sigma_N^4 \text{Trace} \{[\mathbf{D}_1(\theta_0) \mathbf{A}_{20} - \mathbf{D}_2(\theta_0) \mathbf{A}_{10}]^2\}. \quad (59)$$

Hence, (53) becomes (60), shown at the bottom of the next page. Recall that, for  $\theta_S = 0$ ,  $\mathbf{u}_S = 0$ ,  $\mathbf{A}_{11} = (\sigma_S^2/\sigma_N^2) \mathbf{1} \mathbf{1}^T + \mathbf{A}_{10}$ , and  $\mathbf{A}_{21} = \mathbf{A}_{20}$ . If the array is steered to broadside, then  $\mathbf{D}_2(0) = 0$ , and the numerator in (60) becomes

$$\langle b(\theta_0)|H_1 \rangle - \langle b(0)|H_0 \rangle = \sigma_S^2 \text{Trace}(\mathbf{D}_1(0) \mathbf{1} \mathbf{1}^T) \\ - \sigma_S^2 \mathbf{1}^T \mathbf{D}_1(0) \mathbf{1} \\ = \sigma_S^2 \left[ h(0) + 2 \sum_{p=1}^{M-1} h(p) \right]. \quad (61)$$

<sup>1</sup>See [17, problem A.3.6] for the complex version.

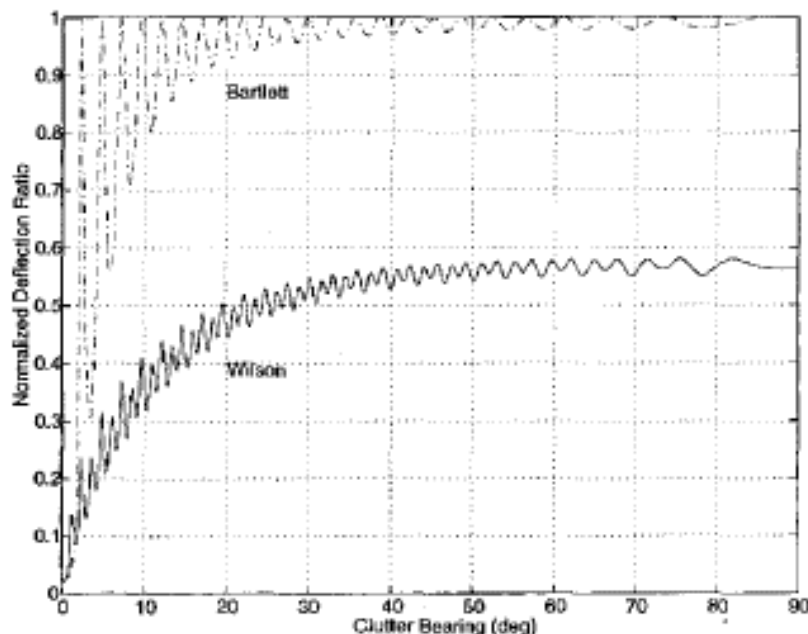


Fig. 4. Normalized deflection ratio for Bartlett and Wilson weights as a function of relative clutter bearing for an INR of 0 dB.

This agrees with previous analysis [2]. Note that the  $\text{Trace}[\mathbf{D}(0)\mathbf{A}_{20}] \leq 0$ . Finally, the expression for the deflection ratio with the array steered to broadside is given by

$$D_f(0, 0) = \frac{\text{SNR} [\mathbf{1}^T \mathbf{D}_1(0) \mathbf{1}]}{\sqrt{\text{Trace}[(\mathbf{D}_1(0)\mathbf{A}_{10})^2] - \text{Trace}[(\mathbf{D}_1(0)\mathbf{A}_{20})^2]}} \quad (62)$$

#### B. Deflection Ratio Comparison: Wilson versus Bartlett Weights

Using (62), a MATLAB program was developed to calculate the normalized deflection ratio under a variety of SNR and INR conditions with and without clutter. The deflection ratio is normalized relative to its maximum value for all weight sequences evaluated and is therefore independent of SNR. When clutter is not present, the deflection ratio reduces to that of a signal in independent noise and the results obtained are identical to those obtained previously [2], i.e., the normalized deflection ratio for a beamformer with Bartlett weights outperforms the beamformer with Wilson weights.

When a clutter signal is present, the normalized deflection ratio is a function of INR and the clutter bearing. Fig. 4 presents a plot of the normalized deflection ratio as a function of clutter bearing for an INR of 0 dB. Fig. 5 is similar but for an INR of 5 dB. It is obvious from the figures that the GCBF with

Bartlett weights outperforms the GCBF with Wilson weights for all clutter bearings except bearings within approximately  $3^\circ$  of the signal bearing.

#### C. Receiver Operating Characteristic Curves: Wilson versus Bartlett Weights

Using MATLAB to numerically integrate (52) and generate true GCBF output pdf's, ROC curves for any given threshold  $\kappa$  can be obtained from the probability of detection (pd) and the probability of false alarm (pfa) expressions given by

$$\text{pd} = \int_{\kappa}^{\infty} p(b|H_1) \text{dB} \quad (63)$$

and

$$\text{pfa} = \int_{\kappa}^{\infty} p(b|H_0) \text{dB}. \quad (64)$$

This procedure allows for a comparison of the detection performance of the GCBF with the two different weight sets. Figs. 6 and 7 show a comparison of detection probabilities for Bartlett and Wilson weight sequences for different clutter bearings for a pfa of 0.01. For both cases, the beamformer maximum response axis and the signal are at broadside and the SNR is 0 dB. In Fig. 6, the INR is 0 dB, while in Fig. 7 the INR is 5 dB. Once again, it is obvious from these figures that the GCBF with Bartlett weights outperforms the GCBF with Wilson weights for all clutter bearings except those close to the look direction.

$$D_f(\theta_0, \theta_S) = \frac{\text{Trace}[\mathbf{D}_1(\theta_0)\mathbf{A}_{11} - \mathbf{D}_2(\theta_0)\mathbf{A}_{21}] - \text{Trace}[\mathbf{D}_1(\theta_0)\mathbf{A}_{10} - \mathbf{D}_2(\theta_0)\mathbf{A}_{20}]}{\sqrt{\text{Trace}\{[\mathbf{D}_1(\theta_0)\mathbf{A}_{10} - \mathbf{D}_2(\theta_0)\mathbf{A}_{20}]^2\} - \text{Trace}\{[\mathbf{D}_1(\theta_0)\mathbf{A}_{20} - \mathbf{D}_2(\theta_0)\mathbf{A}_{10}]^2\}}} \quad (60)$$

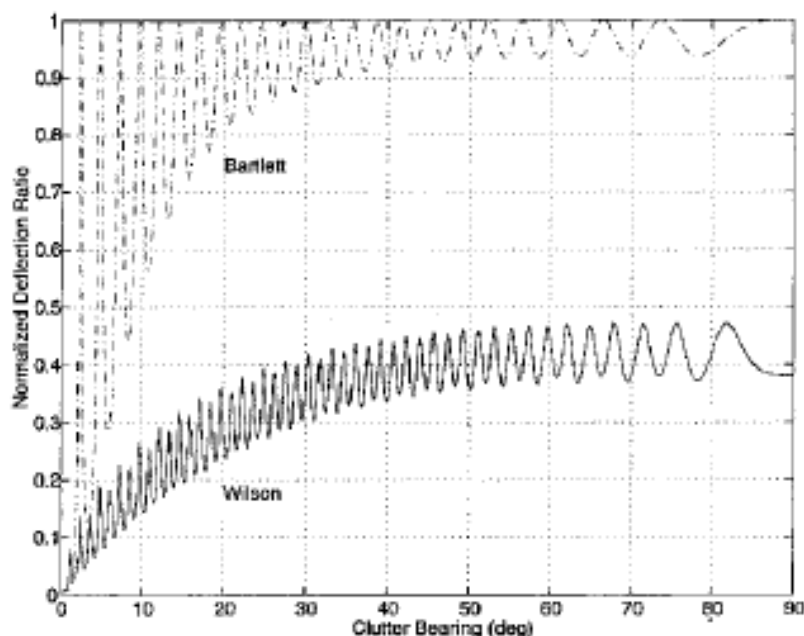


Fig. 5. Normalized deflection ratio for Bartlett and Wilson weights as a function of relative clutter bearing for an INR of 5 dB.

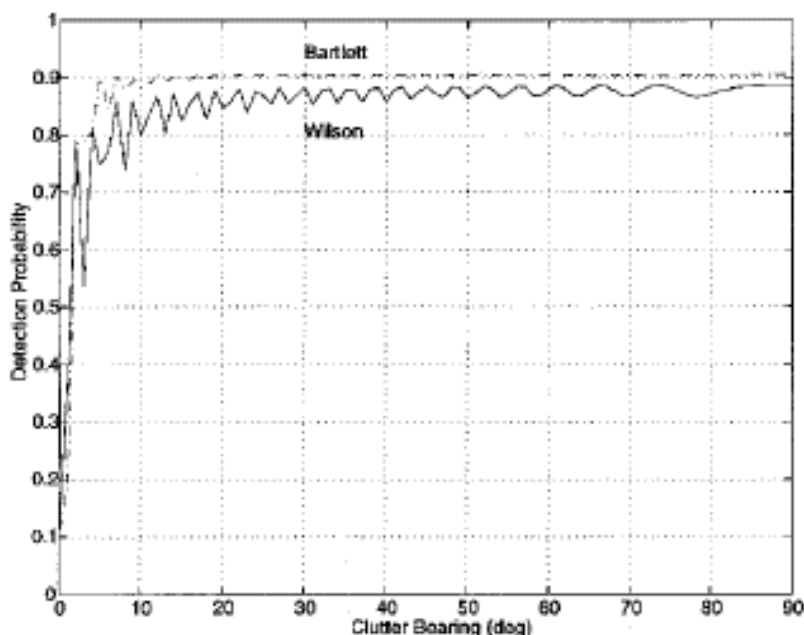


Fig. 6. ROC curves for Bartlett and Wilson weights with  $\text{INR} = \text{SNR} = 0$  and  $p_{fa} = 0.01$ .

However, even near the look direction, the GCBF detection performance with Bartlett weights is close to that of the beamformer with Wilson weights.

#### V. BEARING ESTIMATION OF THE GCBF

The estimation of signal bearing is a two-step process. First, the signal must be detected, i.e., for bearing estimation,  $H_1$  is always true and the signal bearing is chosen as the main response axis of the beam with the largest power output. For high

SNR's, the detection process will result in the selection of the appropriate beam (the beam containing the signal). Normally, the Cramer-Rao bound is computed to generate a lower bound on the rms bearing error. However, the Cramer-Rao bound is based on a likelihood function, and the GCBF is suboptimal in the presence of clutter signals and does not follow from a likelihood ratio formulation. An alternate local rms bearing error bound is developed in Section V-A. Comparison of the local rms bearing estimation errors for Wilson and Bartlett weights will be presented in Section V-B. At a low SNR, it is difficult to choose

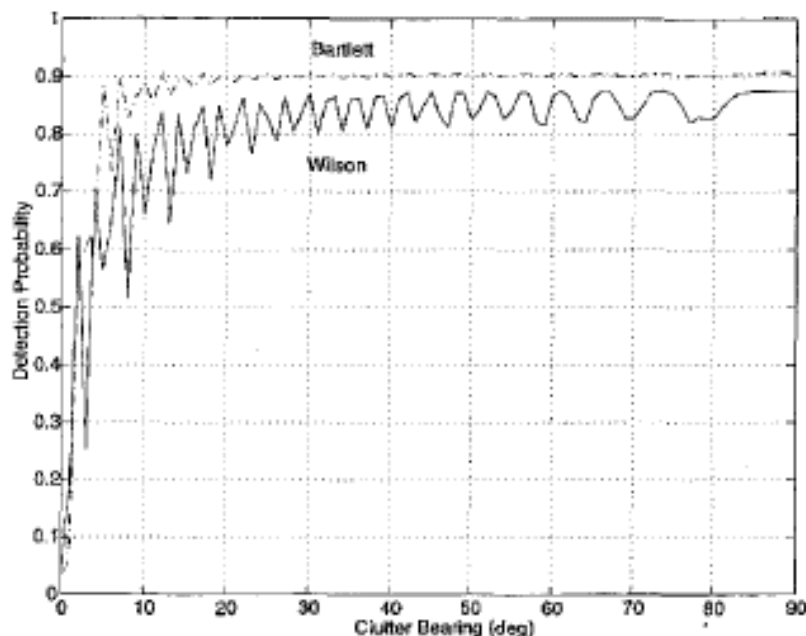


Fig. 7. ROC curves for Bartlett and Wilson weights with INR = 5 dB, SNR = 0, and Pfa = 0.01.

the correct beam containing the signal. For this case, all beams are equally probable and the probability of choosing any beam can be modeled as a uniform distribution over beam space. For this case, the Ziv–Zakai bound is the best global lower bound on the rms bearing error [15]. The development of this lower bound is presented in Section V-C, with a comparison of the results for the two weight sequences presented in Section V-D.

#### A. Lower Bounds on the RMS Bearing Error for Signal Bearings Local to the Beamformer Look Direction

We assume that the signal bearing  $\theta_S$  is in the local vicinity of  $\theta_0$ . Examination of (30) allows us to write  $b(\theta_0, \mathbf{x}(\theta_S)) = \mathbf{x}^T(\theta_S)D(\theta_0)\mathbf{x}(\theta_S)$ . For each random sample of  $\mathbf{x}$ , labeled  $\xi$ , the error in an estimate of the signal bearing can be determined by finding a value of  $\theta_0$  that maximizes  $b$ . That is, find a  $\theta_0$  such that

$$V(\theta_0; \xi) \equiv \partial b(\theta_0; \xi) / \partial \theta_0 = 0. \quad (65)$$

Now, for a fixed  $\xi$ , expand  $b$  in a Taylor series in the neighborhood around the signal bearing

$$b(\theta_0; \xi) = b(\theta_S; \xi) + b'(\theta_S; \xi)(\theta_0 - \theta_S) + \frac{1}{2}b''(\theta_S; \xi)(\theta_0 - \theta_S)^2 + \dots \quad (66)$$

where  $b^{(n)}(\theta_S; \xi)$  is  $b^{(n)}(\theta_0; \xi)$  evaluated at  $\theta_0 = \theta_S$ . Differentiating (66) with respect to  $\theta_0$ , using (65), and ignoring terms higher than first order in  $(\theta_0 - \theta_S)$  yields the bearing estimation error

$$\theta_0 - \theta_S \simeq -V(\theta_S; \xi) / b''(\theta_S; \xi). \quad (67)$$

Denote the expectation over the random variable  $\xi$  as  $\langle \cdot \rangle \equiv E_{\xi}(\cdot)$ . For large  $M$ ,  $\text{Var}_{\xi}(b'') \ll |b''|$ , and we can replace  $b''$  by  $\langle b'' \rangle$  in (67). Thus, we can now write

$$(\theta_0 - \theta_S) \simeq -\frac{\langle b'(\theta_S; \xi) \rangle}{\langle b''(\theta_S; \xi) \rangle}. \quad (68)$$

The variance of the bearing estimate is given by

$$\begin{aligned} \text{Var}(\theta_0 - \theta_S) &= \langle (\theta_0 - \theta_S)^2 \rangle - \langle \theta_0 - \theta_S \rangle^2 \\ &\simeq \frac{\langle [b'(\theta_S; \xi)]^2 \rangle - \langle b'(\theta_S; \xi) \rangle^2}{\langle b''(\theta_S; \xi) \rangle^2} \\ &\simeq \text{Var}(b'(\theta_S; \xi)) / \langle b''(\theta_S; \xi) \rangle^2. \end{aligned} \quad (69)$$

It is easy to show that the Cramer–Rao lower bound on the bearing estimation error for an optimal beamformer reduces to (69) [16].

Now, since  $\mathbf{x}$  is not a function of  $\theta_0$ , from (30) we can write

$$b'(\theta_0) = \mathbf{x}^T D'(\theta_0) \mathbf{x} \quad (70)$$

with

$$D'(\theta_0) = \begin{pmatrix} D'_1(\theta_0) & D'_2(\theta_0) \\ -D'_2(\theta_0) & D'_1(\theta_0) \end{pmatrix}. \quad (71)$$

Here,  $D'_i(\theta_0) \equiv \partial D_i(\theta_0) / \partial \theta_0$ . Then,  $D'_1(\theta_0)$  is a symmetric Toeplitz matrix with elements

$$\begin{aligned} d'_{1p}(\theta_0) &\equiv \frac{\partial d_{1p}(\theta_0)}{\partial \theta_0} \\ &= -kp \cos(\theta_0) d_{2p}(\theta_0) \end{aligned} \quad (72)$$

and  $D'_2(\theta_0)$  is a skew symmetric Toeplitz matrix with elements

$$\begin{aligned} d'_{2p}(\theta_0) &\equiv \frac{\partial d_{2p}(\theta_0)}{\partial \theta_0} \\ &= kp \cos(\theta_0) d_{1p}(\theta_0). \end{aligned} \quad (73)$$

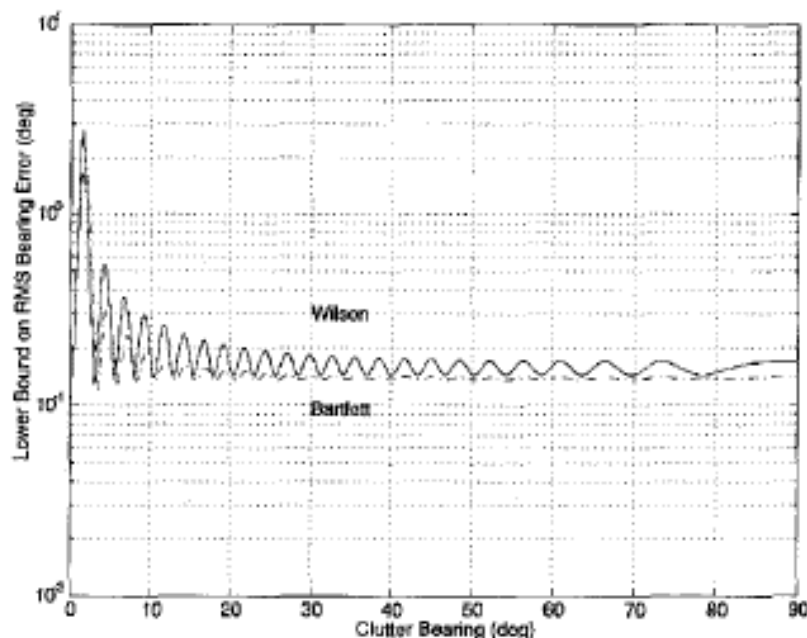


Fig. 8. RMS bearing error for SNR = INR = 0 dB.

$D_1'(\theta_0)$  is symmetric because  $p \cdot d_{2p}(\theta_0)$  is even in  $p$ , and  $D_2'(\theta_0)$  is skew symmetric because  $p \cdot d_{1p}(\theta_0)$  is odd in  $p$ .

Similarly,

$$b'(\theta_0) = \mathbf{x}^T D'(\theta_0) \mathbf{x} \quad (74)$$

with

$$D'(\theta_0) = \begin{pmatrix} D_1'(\theta_0) & D_2'(\theta_0) \\ -D_2'(\theta_0) & D_1'(\theta_0) \end{pmatrix} \quad (75)$$

where  $D_1'(\theta_0)$  is a symmetric Toeplitz matrix with elements

$$d_{1p}'(\theta_0) = kp \sin(\theta_0) d_{2p}(\theta_0) - k^2 p^2 \cos^2(\theta_0) d_{1p}(\theta_0) \quad (76)$$

and  $D_2'(\theta_0)$  is a skew symmetric Toeplitz matrix with elements

$$d_{2p}'(\theta_0) = -kp \sin(\theta_0) d_{1p}(\theta_0) - k^2 p^2 \cos^2(\theta_0) d_{2p}(\theta_0). \quad (77)$$

In a manner similar to the development of (60), (69) becomes

$$\begin{aligned} \text{Var}(\theta_0 - \theta_S) &= \frac{\text{Trace} \{ [D_1'(\theta_S) \mathbf{A}_{11}(\theta_S) - D_2'(\theta_S) \mathbf{A}_{21}(\theta_S)]^2 \}}{[\text{Trace} \{ D_1'(\theta_S) \mathbf{A}_{11}(\theta_S) - D_2'(\theta_S) \mathbf{A}_{21}(\theta_S) \}]^2} \\ &\quad - \frac{\text{Trace} \{ [D_1'(\theta_S) \mathbf{A}_{21}(\theta_S) - D_2'(\theta_S) \mathbf{A}_{11}(\theta_S)]^2 \}}{[\text{Trace} \{ D_1'(\theta_S) \mathbf{A}_{11}(\theta_S) - D_2'(\theta_S) \mathbf{A}_{21}(\theta_S) \}]^2}. \quad (78) \end{aligned}$$

If the signal is at array broadside and there is no clutter, (78) reduces to

$$\text{Var}(\theta_0 - \theta_S)|_{\theta_S \rightarrow 0} = -\frac{\text{Trace} \{ [D_2'(0) \mathbf{1} \mathbf{1}^T]^2 \}}{[\mathbf{1}^T D_1'(0) \mathbf{1}]^2}. \quad (79)$$

The rms bearing error for the GCBF in the absence of clutter with the signal arriving from broadside is thus given by the square root of the variance of the bearing error shown in (79).

### B. Comparison of Local RMS Bearing Errors for Wilson and Bartlett Weights

When clutter is not present, the rms bearing error calculated from (79) is constant, with the error associated with using the Wilson correlation-weight sequence exceeding that associated with using the Bartlett correlation-weight sequence by 0.03 degrees. When clutter is present, the local rms bearing errors calculated from (78) for a continuum of clutter bearings are shown in Figs. 8 and 9. For both figures, the signal direction is 0 degrees, the SNR is 0 dB, and the INR is 0 and 5 dB, respectively. As the figures show, the rms bearing error for the GCBF with Wilson weights is greater than it is for Bartlett weights for almost all clutter bearings. The bearing errors associated with using the Wilson correlation-weight sequence also oscillate more due to higher sidelobe levels.

### C. Global Lower Bounds on the RMS Bearing Error

For low SNR's, it can no longer be assumed that the signal bearing necessarily corresponds to the beam with the maximum power output. Therefore, there is a finite probability that the wrong beam will be chosen. It is obvious that the corresponding rms bearing errors will be much larger where the local error bounds developed in the previous subsection no longer apply. Under these circumstances, the Ziv-Zakai bound [15] will give a more accurate depiction of the rms bearing error, especially if a peakpicker is used in conjunction with the postbeamformer detection process. It should be noted that the Ziv-Zakai bound developed here is independent of the true signal bearing.

For a multibeam process utilizing a peakpicker, we can examine a simple hypothesis test for detection/bearing estimation. Consider a two-state hypothesis test that uses the

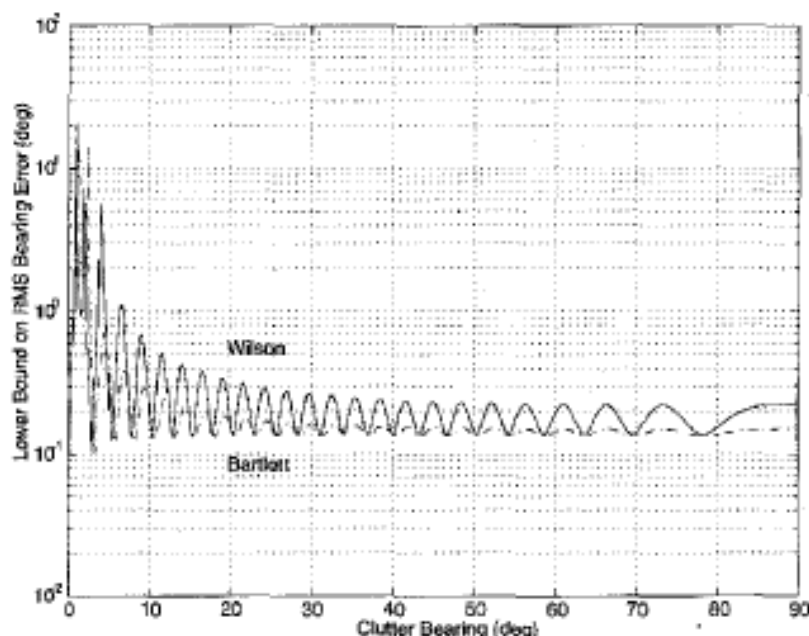


Fig. 9. RMS bearing error for SNR = 0 dB and INR = 5 dB.

beamformed output of two beams to generate an estimate  $\hat{\theta}$  of the signal bearing, where the MRA of one of two beams must be chosen:

$$\begin{aligned} H_1: \hat{\theta} &= \theta_0 \\ H_0: \hat{\theta} &= \theta_0 + \vartheta. \end{aligned} \quad (80)$$

Under  $H_1$ , the bearing estimate is  $\theta_0$ , while under  $H_0$  the estimate is  $\theta_0 + \vartheta$ . Note that  $\theta_0$  and  $\theta_0 + \vartheta$  represent the maximum response axes of two beams which may not be adjacent. When only a portion of the beams available need to be considered as candidates for the beam containing the signal, it can be assumed that  $\theta_{\min} \leq \theta \leq \theta_{\max}$  (ignoring any bearing ambiguities due to array geometry). When  $\theta_{\max} < \pi/2$  and/or  $\theta_{\min} > -\pi/2$ , the set of beams chosen will be referred to as a set of *skint* beams. Now, consider the case where  $\theta_{\max} = \pi/2$  and  $\theta_{\min} = -\pi/2$ , i.e.,  $\hat{\theta}$  can take on any value over the range  $-\pi/2 \leq \hat{\theta} \leq \pi/2$ . Both  $\theta_0$  and  $\theta_0 + \vartheta$  can fall anywhere in the same range as  $\hat{\theta}$ . If we assume that  $\theta_0 < \theta_0 + \vartheta$ , it follows that  $-\pi/2 \leq \theta_0 \leq \pi/2 - \vartheta$ , with  $-\pi/2 < \vartheta \leq \pi/2$ .

A suboptimal estimation strategy (binary peakpicker) could be of the form

$$b(\theta_0) \underset{H_1}{\overset{H_0}{>}} b(\theta_0 + \vartheta). \quad (81)$$

If it is assumed that  $H_1$  and  $H_0$  are equally likely, i.e.,  $P(H_1) = P(H_0) = 1/2$ , the probability of choosing the incorrect beam can be written as

$$P(\text{error}) = \frac{1}{2} P(\hat{\theta} > \theta_0 + \vartheta/2 | H_1) + \frac{1}{2} P(\hat{\theta} < \theta_0 + \vartheta/2 | H_0) \quad (82)$$

but (81) generates a suboptimum estimate for  $\hat{\theta}$ . Therefore, the bearing error probability is bounded from below by the minimum error probability  $P_e(\theta_0, \theta_0 + \vartheta)$  for the optimal estimator, given by

$$P_e(\theta_0, \theta_0 + \vartheta) \leq \frac{1}{2} P(\epsilon > \vartheta/2 | \theta_0) + \frac{1}{2} P(\epsilon < -\vartheta/2 | \theta_0 + \vartheta) \quad (83)$$

where  $\epsilon$  is the error in the estimate of  $\hat{\theta}$ , given by  $\epsilon \equiv \hat{\theta} - \theta_0$  under  $H_1$ , or  $\epsilon \equiv \hat{\theta} - (\theta_0 + \vartheta)$  under  $H_0$ . The notation  $|\theta_0$  and  $|\theta_0 + \vartheta$  denote  $H_1$  and  $H_0$ , respectively. This notation will be used interchangeably.

Integrating (83) over the limits of  $\theta_0$  leads to

$$\int_{-\pi/2}^{\pi/2 - \vartheta} P_e(\theta_0, \theta_0 + \vartheta) d\theta_0 \leq \frac{1}{2} \int_{-\pi/2}^{\pi/2} P(|\epsilon| > \vartheta/2 | \theta_0) d\theta_0. \quad (84)$$

Defining

$$F(\vartheta) \equiv \frac{1}{\pi} \int_{-\pi/2}^{\pi/2} P(|\epsilon| > \vartheta | \theta_0) d\theta_0 \quad (85)$$

then

$$\int_{-\pi/2}^{\pi/2 - \vartheta} P_e(\theta_0, \theta_0 + \vartheta) d\theta_0 \leq \left(\frac{\pi}{2}\right) F(\vartheta/2). \quad (86)$$

Multiplying both sides by  $2\vartheta/\pi$  and integrating over  $\vartheta$ , and using the fact that  $P(|\epsilon| > \vartheta | \theta_0) = 1$  for  $\vartheta \leq 0$  yields

$$\begin{aligned} (2/\pi) \int_{-\pi/2}^{\pi/2} \int_{-\pi/2}^{\pi/2 - \vartheta} \vartheta P_e(\theta_0, \theta_0 + \vartheta) d\theta_0 d\vartheta \\ \leq -2 \int_0^{\pi} s^2 F'(s) ds \end{aligned} \quad (87)$$

where  $s = \theta/2$ . Now, we examine  $F'(s)$  as follows:

$$\begin{aligned} F'(s) &= \lim_{\delta s \rightarrow 0} \frac{1}{\pi} \int_{-\pi/2}^{\pi/2} [P(|\epsilon| > s + \delta s|\theta_0) \\ &\quad - P(|\epsilon| > s|\theta_0)] \frac{d\theta_0}{\delta s} \\ &= - \lim_{\delta s \rightarrow 0} \frac{1}{\pi} \int_{-\pi/2}^{\pi/2} P(|\epsilon| - \delta s < s < |\epsilon| |\theta_0) \frac{d\theta_0}{\delta s} \\ &= - \frac{1}{\pi} \int_{-\pi/2}^{\pi/2} P(s|\theta_0) d\theta_0 \end{aligned} \quad (88)$$

where  $P(s|\theta_0)$  is the pdf of the error  $\epsilon$  conditioned on  $\theta_0$ . Thus,  $-F'(s)$  is the unconditional pdf of  $\epsilon$ , assuming that the prior pdf of  $\hat{\theta}$  is uniform on  $[-\pi/2, \pi/2]$ .

Therefore, the bearing error variance  $\sigma_\epsilon^2$  is given by

$$\sigma_\epsilon^2 = - \int_0^\pi s^2 F'(s) ds \quad (89)$$

and using (87) in (89) results in the Ziv-Zakai bound on the bearing estimation errors

$$\sigma_\epsilon^2 \geq \frac{1}{\pi} \int_{-\pi/2}^{\pi/2} \vartheta d\vartheta' \int_{-\pi/2}^{\pi/2-\vartheta} P_\epsilon(\theta_0, \theta_0 + \vartheta) d\theta_0. \quad (90)$$

Since a likelihood function does not exist for the beamformer in the presence of clutter, an expression for  $P_\epsilon(\theta_0, \theta_0 + \vartheta)$  must now be developed. Define the sufficient statistic for the output of a beamformer steered to bearing  $\theta_0$  as

$$\begin{aligned} l &\triangleq b(\theta_0) - b(\theta_0 + \vartheta) \\ &= \mathbf{x}^T \mathbf{D}(\theta_0) \mathbf{x} - \mathbf{x}^T \mathbf{D}(\theta_0 + \vartheta) \mathbf{x}. \end{aligned} \quad (91)$$

Choose  $H_1(\hat{\theta} = \theta_0)$  if  $l \geq 0$  and  $H_0(\hat{\theta} = \theta_0 + \vartheta)$  if  $l < 0$ . Clearly, the test chooses the largest peak. Note that the case  $l < 0$  under  $H_1$  or  $l \geq 0$  under  $H_0$  constitute error conditions. Therefore, if the corresponding pdf's  $p(l|H_0)$  and  $p(l|H_1)$  are known, then

$$P_\epsilon(\theta_0, \theta_0 + \vartheta) \simeq \frac{1}{2} \int_{-\infty}^0 p(l|\theta_0) dl + \frac{1}{2} \int_0^\infty p(l|\theta_0 + \vartheta) dl. \quad (92)$$

Since  $\Phi(\omega|H_i)$  is the characteristic function of  $p(l|H_i)$ ,

$$p(l|H_0) = \frac{1}{2\pi} \int_{-\infty}^{\infty} \Phi(\omega|H_0) e^{j\omega l} d\omega. \quad (93)$$

Substitution of (93) into (92) and integration over  $l$  is not possible because the integral over  $l$  and  $\omega$  cannot be interchanged. Let  $s = c_q + j\omega$ , where  $c_q$  is a constant, and let  $\Phi(\omega|H_q) = \psi(s|H_q) e^{c_q l}$ ; then  $p(l|H_q)$  will be expressed in terms of the inverse Laplace transform (Bromwich integral or Fourier-Mellin integral) of  $\psi(s|H_q)$  [14], [15] as

$$p(l|H_q) = \frac{1}{2\pi j} \int_{c_q - j\infty}^{c_q + j\infty} \psi(s|H_q) e^{sl} ds. \quad (94)$$

The integration path, called the Bromwich path, is for a constant value of  $c_q$  and for  $-\infty < \omega < \infty$ .

Consider the first integral in (94) for  $l < 0$ . The constant  $c_1$  must be chosen such that  $0 < c_1 < \text{Min}(p_1^{1+})$  where

$$p_1^{1+} = \{\text{Re}(\text{poles of } \psi(s|H_1)) | \text{Re}(s) > 0\}. \quad (95)$$

That is, the Bromwich path must be to the left of all poles corresponding to  $\psi(s|H_1)$  on the positive  $\text{Re}(s)$  axis. The condition  $c_1 > 0$  assures that the order on integration can be switched. Thus

$$\begin{aligned} \int_{-\infty}^0 p(l|\theta_0) dl &= \frac{1}{2\pi j} \int_{-\infty}^0 \int_{c_1 - j\infty}^{c_1 + j\infty} \psi(s|H_1) e^{sl} ds dl \\ &= \frac{1}{2\pi j} \int_{c_1 - j\infty}^{c_1 + j\infty} \frac{\psi(s|H_1)}{s} ds \\ &= \frac{1}{2\pi} \int_{-\infty}^{\infty} \frac{\psi(c_1 + j\omega|H_1)}{c_1 + j\omega} d\omega. \end{aligned} \quad (96)$$

Similarly, for  $l \geq 0$ ,  $c_0$  must be chosen such that  $\text{Max}(p_0^{0-}) < c_0 < 0$  where

$$p_0^{0-} = \{\text{Re}(\text{poles of } \psi(s|H_0)) | \text{Re}(s) < 0\}. \quad (97)$$

Then, the second integral in (92) becomes

$$\begin{aligned} \int_0^\infty p(l|\theta_0) dl &= \frac{1}{2\pi j} \int_0^\infty \int_{c_0 - j\infty}^{c_0 + j\infty} \psi(s|H_0) e^{sl} ds dl \\ &= - \frac{1}{2\pi j} \int_{c_0 - j\infty}^{c_0 + j\infty} \frac{\psi(s|H_0)}{s} ds \\ &= - \frac{1}{2\pi} \int_{-\infty}^{\infty} \frac{\psi(c_0 + j\omega|H_0)}{c_0 + j\omega} d\omega. \end{aligned} \quad (98)$$

Note that the condition that the Bromwich path must be to the left or right of the corresponding singularities follows from the Cauchy integral theorem [14].

Therefore, (92) becomes

$$\begin{aligned} P_\epsilon(\theta_0, \theta_0 + \vartheta) &\simeq \frac{1}{4\pi} \int_{-\infty}^{\infty} \frac{\psi(c_1 + j\omega|H_1)}{c_1 + j\omega} d\omega \\ &\quad - \frac{1}{4\pi} \int_{-\infty}^{\infty} \frac{\psi(c_0 + j\omega|H_0)}{c_0 + j\omega} d\omega. \end{aligned} \quad (99)$$

Noting the analogy of (91) to (30), we can obtain by analogy with (46)

$$\Phi_{l(\theta_0, \theta_0 + \vartheta)}(\omega|H_q) = |I + 2j\omega[D(\theta_0) - D(\theta_0 + \vartheta)]R_1(\theta_S)|^{-1/2}. \quad (100)$$

By analogy with (49), we make use of the singular value decomposition of  $[D(\theta_0)D(\theta_0 + \vartheta)]R_1(\theta_S) = U_1 \Lambda(\theta_0; \theta_S) V_1^T$ , which, by analogy with (51), leads to

$$\Phi_{l(\theta_0, \theta_0 + \vartheta)}(\omega|H_q) = \prod_{k=1}^{2M} \left( \frac{1}{1 + 2j\omega \lambda_k(\theta_0; \theta_S)} \right)^{1/2}. \quad (101)$$

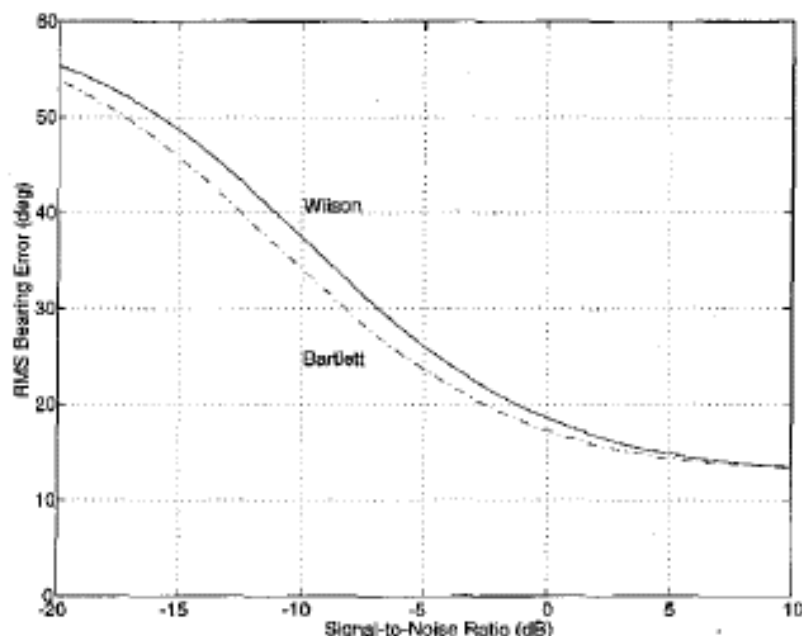


Fig. 10. Ziv-Zakai lower bound on rms bearing error as a function of SNR for signal plus noise delay.

Thus,

$$\begin{aligned}
 P_e(\theta_0, \theta_0 + \vartheta; \theta_S) & \\
 & \approx \frac{1}{4\pi} \int_{-\infty}^{\infty} \frac{1}{c_1 + j\omega} \prod_{k=1}^{2M} \left( \frac{1}{1 + 2j(c_1 + j\omega)\lambda_k(\theta_0; \theta_S)} \right)^{1/2} d\omega \\
 & \quad - \frac{1}{4\pi} \int_{-\infty}^{\infty} \frac{1}{c_0 + j\omega} \\
 & \quad \cdot \prod_{k=1}^{2M} \left( \frac{1}{1 + 2j(c_0 + j\omega)\lambda_k(\theta_0 + \vartheta; \theta_S)} \right)^{1/2} d\omega. \quad (102)
 \end{aligned}$$

Using (102) in (90) results in an approximate lower bound for  $\sigma_e^2$ .

#### D. Comparison of Global RMS Bearing Errors for Wilson and Bartlett Weights

Results from the computation of the Ziv-Zakai lower bound on bearing estimation error for  $-\pi/2 \leq \hat{\theta} \leq \pi/2$  are shown in Figs. 10–12. Fig. 10 illustrates the Ziv-Zakai lower bound on the rms bearing error for the signal plus noise only case (no clutter). It shows that, as SNR decreases, the lower bound for both Bartlett and Wilson weights approaches that of the rms error associated with an error that is uniformly distributed over 180 degrees. Figs. 11 and 12 illustrate the lower bound on the rms bearing error for INR's of 0 and 5 dB, respectively, with the SNR at 0 dB. Examination of the figures shows that the bearing error bound is always larger for Wilson weights than it is for Bartlett weights and that the effect of a strong clutter signal on the rms bearing error is greater for Wilson weights than it is for Bartlett weights.

For a set of squint beams with  $-10^\circ \leq \hat{\theta} \leq 10^\circ$ , Figs. 13 and 14 correspond to the same SNR and INR of Figs. 11 and 12. It is obvious from the figures that reducing the allowable bearing range for the signal improves the lower bound on the

rms bearing error. However, the Bartlett weights still outperform the Wilson weights at almost all clutter bearings.

## VI. SUMMARY AND CONCLUSIONS

In this paper, a generalized quadratic form of the GCBF was proposed and detection and bearing estimation performance metrics were developed for an arbitrary correlation-weight sequence. Two classes of correlation-weight sequences can be used with the GCBF: those that can be generated from real element-weight sequences through a convolution operation and those that cannot. For performance comparison purposes, the simplest examples of each class of correlation-weight sequences were used, Bartlett triangular correlation-weights (which can be generated from a convolution of the unity element-weight sequence), and Wilson unity correlation-weights. Two conclusions were drawn concerning the beamformer responses for the two weight sets: Wilson weights result in a more oscillatory response than Bartlett weights, with a negative response for many bearings, and Wilson weights have a narrower main lobe response than that of the Bartlett weights. The first conclusion implies that there is an increase in sidelobe leakage at many bearings for the Wilson weights and thus a potential for a decrease in detection capability when clutter is present in the sidelobes. The second conclusion gives the GCBF response with Wilson weights a better resolution in the look direction and the ability to resolve closely spaced targets. This appears to be the primary advantage to be gained from using Wilson weights versus the more conventional weights.

Single snapshot beamformer responses for the case of two deterministic signals show that the GCBF with Wilson correlation-weights contain spurious peaks at look directions between the bearings of the two signals. These spurious peaks arise from cross terms in the beamformer equations for look directions between the two signal bearings. For Bartlett correlation-weights,

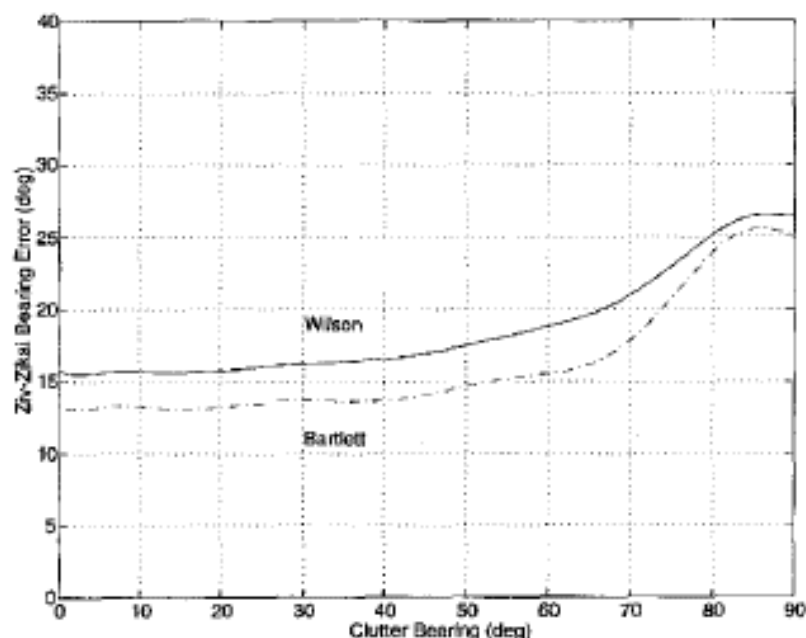


Fig. 11. Smoothed Ziv-Zakai lower bound on bearing error for  $\text{SNR} = \text{INR} = 0$  dB.

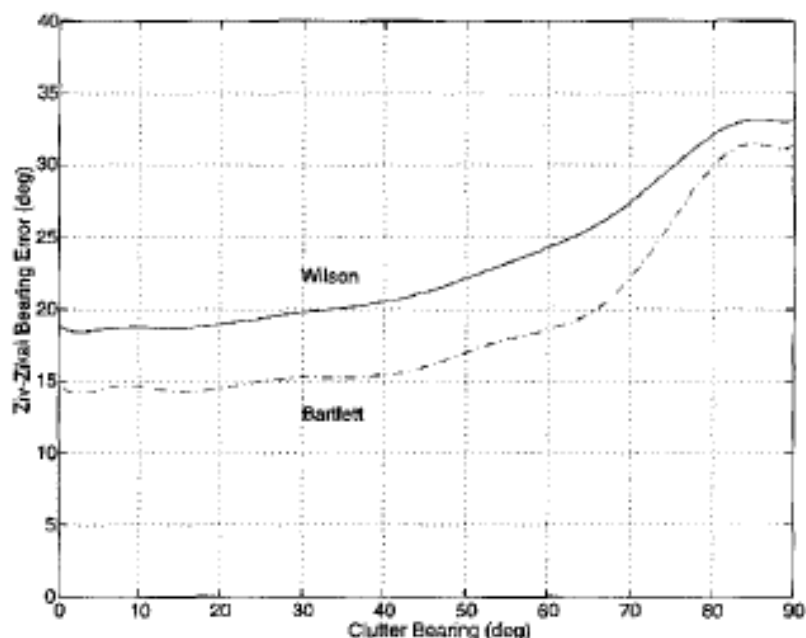


Fig. 12. Smoothed Ziv-Zakai lower bound on bearing error for  $\text{SNR} = 0$  dB and  $\text{INR} = 5$  dB.

the weights act as a spatial filter that minimizes the impact of the cross terms by suppression of the sidelobe response.

General expressions for the pdf of the output of the GCBF were then developed in terms of the inverse Fourier transform of the characteristic function. The noise model for these general expressions included element-to-element independent noise and spatially discrete interferers (clutter.) For the case where no clutter signals are present, closed-form solutions for the pdf could be obtained for both Bartlett and Wilson weight sets [16]. For Bartlett weights, the GCBF output pdf for the noise-only case is a  $\chi^2$  distribution with two degrees of freedom. For

Wilson weights, the output pdf for the noise-only case is a mixture distribution composed of a weighted sum of symmetric  $\chi^2$  distributions, each with two degrees of freedom.

Analytical performance measures were then developed for the GCBF for both detection and bearing estimation. For detection, general expressions for the deflection ratio were generated, and the normalized deflection ratio was calculated for both weight sets. When clutter is absent, the Bartlett weight set outperforms the Wilson weight set at all SNR's. When clutter is present, the Bartlett weights outperform the Wilson weights except when the clutter signal is very close to the look direction,

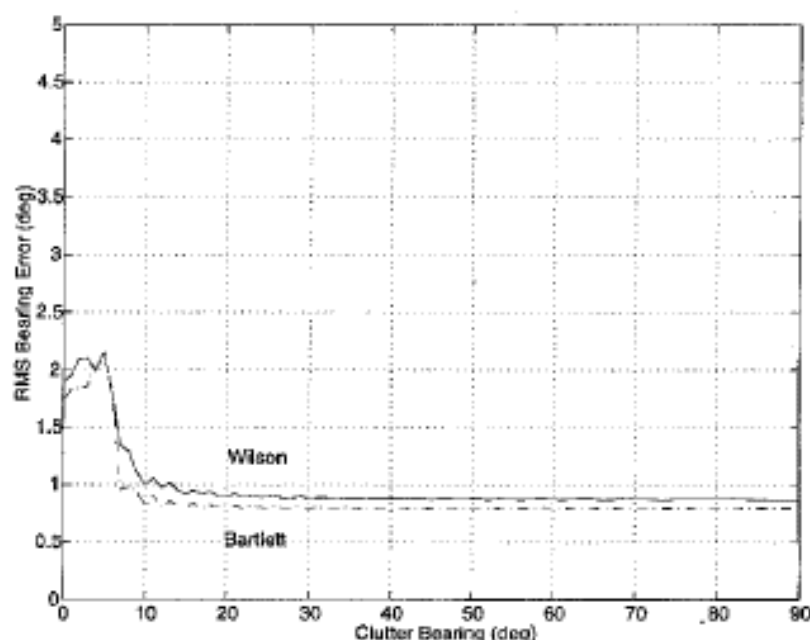


Fig. 13. Smoothed squint beam Ziv-Zakai lower bound on squint beam bearing error for  $SNR = INR = 0$  dB.

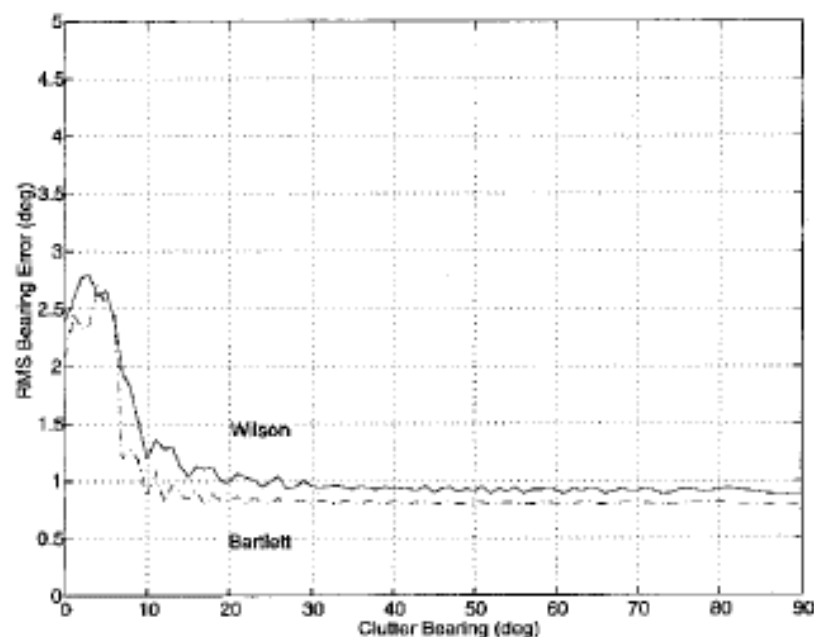


Fig. 14. Smoothed squint beam Ziv-Zakai lower bound on squint beam bearing error for  $SNR = 0$  dB and  $INR = 5$  dB.

where the higher resolution provided by the Wilson weight set dominates detection by rejecting the clutter signal. Since deflection ratio is not an absolute measure of detection performance for non-Gaussian detector outputs, ROC curves were computed numerically using the general expression for the GCBF pdf. The resulting ROC curves showed results identical to those of the deflection ratio. Bartlett weights outperformed Wilson weights except for close-in clutter.

RMS bearing error bounds were then developed for both the local and global bearing estimators. For local bearing estimator

errors, it was assumed that the correct beam was chosen during detection. For this case, general analytical expressions were developed which allowed for computation of the rms bearing error for both Bartlett and Wilson weights. Once again, the Bartlett weights outperformed the Wilson weights for all clutter bearings except those close to the signal bearing. For global bearing estimation errors, it is assumed that the probability of the detected signal being at any give bearing over a range of bearings is uniformly distributed over that range. For this case, the Ziv-Zakai lower bound gives a better estimate of rms bearing errors than

those of the local estimator bound. General expressions for the Ziv-Zakai bound for the GCBF were developed. Plots of the Ziv-Zakai bounds for a full bearing range of  $\pm 90^\circ$  and for a squint beam range of  $\pm 10^\circ$  show that the Bartlett weights outperformed the Wilson weights for all clutter bearings.

To summarize the performance results:

- the response of a correlation beamformer with Wilson weights when two deterministic signals are present at different bearings will contain spurious peaks at beamformer look directions between the bearings of the two signals due to the presence of cross terms in the correlation function;
- when clutter is absent, the GCBF with Bartlett weights will outperform the GCBF with Wilson weights for both detection (deflection and ROC curves) and bearing estimation (local lower bound on rms bearing error and Ziv-Zakai lower bound);
- when a clutter signal is present, use of the Bartlett weights in the GCBF give better performance than use of the Wilson weights for both detection (deflection and ROC curves) and bearing estimation (local lower bound on rms bearing error and Ziv-Zakai lower bound) for all clutter bearings except those close to the signal bearing. For the more realistic Ziv-Zakai lower bounds, GCBF performance with Wilson weights never exceeds that of the Bartlett weights.

Based on the analysis contained in this report, it can be concluded that, in the presence of clutter signals at any bearing except bearings close to that of the signal of interest, the GCBF with Bartlett weights will outperform the GCBF with Wilson weights for both detection and bearing estimation. The presence of clutter signals in the higher sidelobes of the GCBF with Wilson weights significantly degrades performance and can cause spurious peaks in the beamformer response in look directions where no signal is present. The primary performance gain to be had from using Wilson weights is in resolving closely spaced signals.

Although not considered here, it would be interesting to expand the analysis of this report and compare the performance of the two correlation-weight sequence classes in a more general way.

#### ACKNOWLEDGMENT

The authors are grateful to Dr. D. Knobles and the anonymous reviewers for their constructive comments that led to the enhancement of the quality of this paper.

#### REFERENCES

- [1] R. O. Nielsen, *Sonar Signal Processing*. Boston, MA: Artech House, 1991.
- [2] A. J. Haug and G. M. Jaryna, "Analytical Performance Analysis of the Wilson Beamformer," MITRE Tech Memo WN 97W0000128, December 1997.
- [3] J. H. Wilson, "Application of inverse beamformer theory," *J. Acoust. Soc. Amer.*, vol. 98, no. 6, pp. 3250-3261, 1995.
- [4] S. L. Marple, *Digital Spectral Analysis With Applications*. Englewood Cliffs, NJ: Prentice-Hall, 1987, ch. 4 and 5.
- [5] J. Donald, A. H. Nuttall, and J. H. Wilson, "Inverse Beamforming Sonar System and Method," US Patent Number 5216540, June 1993.
- [6] J. P. Fisher and J. H. Wilson, "Minimum detectable level evaluation of inverse beamforming using outpost SUNRISE data," *J. Acoust. Soc. Amer.*, vol. 98, no. 6, pp. 3262-3278, 1995.
- [7] R. A. Mucci, "A comparison of efficient beamforming algorithms," *IEEE Trans. Acoust., Speech, Signal Processing*, vol. ASSP-32, no. 3, pp. 548-558, 1984.
- [8] K. B. Yu and S. Chang, "Signal synthesis from pseudo-Wigner distributions and applications," *IEEE Trans. Acoust., Speech, Signal Processing*, vol. ASSP-35, pp. 1289-1302, Sept. 1987.
- [9] A. H. Nuttall, "Determination of Noise Field Directionality Directly from Spatial Correlation from Linear, Planar, and Volumetric Arrays," NUSC Technical Report, Oct. 6, 1989.
- [10] ———, "Estimation of Noise Field Directionality: Comparison with Fourier Series Method," NUSC Technical Report, Oct. 15, 1989.
- [11] A. H. Nuttall and J. H. Wilson, "Estimation of the acoustic field directionality by use of planar and volumetric arrays via Fourier series method and Fourier integral method," *J. Acoust. Soc. Am.*, pt. 1, vol. 90, no. 4, pp. 2019-2024, 1991.
- [12] A. Papoulis, *Probability, Random Variables, and Stochastic Processes*. New York, NY: McGraw-Hill, 1965.
- [13] J. G. Proakis, *Digital Communications*, 2nd ed. New York, NY: Academic, 1970.
- [14] G. Arfken, *Mathematical Methods for Physicists*. New York, NY: Academic, 1970.
- [15] E. Weinstein and A. J. Weiss, "Fundamental limitations of passive time-delay estimation—Part II: Wide-band systems," *IEEE Trans. Acoust., Speech, Signal Processing*, vol. ASSP-32, pp. 1064-1078, May 1984.
- [16] A. J. Haug and G. M. Jaryna, "Analytical Performance of Generalized Correlation Beamformers," MITRE Tech Memo MP98W0000131, June 1998.
- [17] H. L. Van Trees, *Detection, Estimation, and Modulation Theory, Part III*. New York, NY: Wiley, 1971.

**Anton J. Haug** was born in Sacramento, CA, on September 23, 1941. He received the B.S. degree from the State University of New York at Stony Brook in 1964, the M.S. degree from the City University of New York at Queens College in 1968, and the Ph.D. degree from the Catholic University of Washington, DC, in 1974, all in physics.

He has held a number of positions in both commercial and not-for-profit organizations, including the John Hopkins University Applied Physics Laboratory, Planning Systems Incorporated, EG&G, Martin Marietta, SAIC, and Intermetrics, all in the greater Washington, DC, area. In addition, he has been retained as a Technical Consultant by numerous firms including Expert Witness Consulting on patent suits and a government contract award dispute. He is currently employed as Division Staff at The MITRE Corporation, Reston, VA. His areas of specialty include active and passive noise and vibration control. He has also consulted on problems in digital communications and coding theory and electromagnetic detection of submarines.

Dr. Haug was the recipient of a Parsons Fellowship while at the John Hopkins University Applied Physics Laboratory which allowed him to conduct research in range-dependent propagation modeling and acoustic scattering theory at Johns Hopkins University during the 1976-1977 academic year. He was also Co-Inventor of the Year in 1987 at the Martin Marietta Middle River plant in Maryland.

**Garry M. Jaryna** received the B.S. degree in physics and the M.S. and Ph.D. degrees in mathematics from Rensselaer Polytechnic Institute, Troy, NY, in 1973, 1974, and 1977, respectively.

He is currently the Consulting Scientist for the Naval Systems and Technology Division of the MITRE Corporation, Reston, VA. His responsibilities include program management as well as extensive research in the areas of sonar system performance modeling, artificial neural networks, wavelet detection and estimation, higher-order spectral analysis, adaptive beamforming, nonlinear control theory, and nonlinear signal modeling. He is also an Adjunct Assistant Professor of Electrical Engineering at The Catholic University, Washington, DC, teaching in areas of communication theory, stochastic processes, sonar signal processing, detection and estimation theory, and neural networks. Prior to joining MITRE in 1987, he was employed at UNISYS, performing EW system studies including wide-band detection, robust localization, direction finding, and signal parameter identification and characterization. He was employed at Planning Systems Incorporated from 1977 to 1984 as a Senior Systems Analyst responsible for the analysis and review of advanced sonar equipment.